ADVANCED FUNCTIONAL MATERIALS
www.afm-journal.de

www.MaterialsViews.com

# A Cruciform Electron Donor–Acceptor Semiconductor with Solid-State Red Emission: 1D/2D Optical Waveguides and Highly Sensitive/Selective Detection of $H_2S$ Gas

*Hewei Luo, Songjie Chen, Zitong Liu,* Chuang Zhang, Zhengxu Cai, Xin Chen, Guanxin Zhang,* Yongsheng Zhao, Silvio Decurtins, Shi-Xia Liu,* and Deqing Zhang**

**In this paper, a new cruciform donor–acceptor molecule 2,2'-((5,5'-(3,7-dicyano-2,6-bis(dihexylamino)benzo[1,2-b:4,5-b']difuran-4,8-diyl)bis(thiophene-5,2-diyl))bis (methanylylidene))dimalononitrile (BDFTM) is reported. The compound exhibits both remarkable solid-state red emission and *p*-type semiconducting behavior. The dual functions of BDFTM are ascribed to its unique crystal structure, in which there are no intermolecular face-to-face $\pi$–$\pi$ interactions, but the molecules are associated by intermolecular CN...$\pi$ and H-bonding interactions. Firstly, BDFTM exhibits aggregation-induced emission; that is, in solution, it is almost non-emissive but becomes significantly fluorescent after aggregation. The emission quantum yield and average lifetime are measured to be 0.16 and 2.02 ns, respectively. Crystalline microrods and microplates of BDFTM show typical optical waveguiding behaviors with a rather low optical loss coefficient. Moreover, microplates of BDFTM can function as planar optical microcavities which can confine the emitted photons by the reflection at the crystal edges. Thin films show an air-stable *p*-type semiconducting property with a hole mobility up to 0.0015 $cm^2V^{-1}s^{-1}$. Notably, an OFET with a thin film of BDFTM is successfully utilized for highly sensitive and selective detection of $H_2S$ gas (down to ppb levels).**

## 1. Introduction

In recent years, conjugated molecules with different structural and functional motifs have been synthesized and investigated with the aim to develop high performance optoelectronic materials.[1,2] In fact, organic semiconductors (*p*-, *n*- and even ambipolar types) with high carrier mobilities have been reported.[3–5] Organic light-emitting materials of high quantum efficiencies have been achieved via different approaches.[6,7] Intermolecular $\pi$–$\pi$ stacking and other interactions are usually present within organic semiconductors to form conducting pathways. However, such intermolecular $\pi$-$\pi$ interactions are detrimental to light-emission because of the formation of excimers or exciplexes. Thus, it seems that it is challenging to obtain dual function molecular materials exhibiting both semiconducting and emissive properties. Notwithstanding, such dual function molecular materials are highly desirable for applications in devices such as light-emitting field-effect transistors. The fine-tuning of intermolecular interactions and structural arrangements is an efficient approach to realize molecular materials with both semiconducting and emissive properties. For instance, Perepichka and co-workers described a semiconductor which simultaneously shows a high mobility (1.0 $cm^2\ V^{-1}\ s^{-1}$) and photoluminescence with a quantum yield of 70% in the crystalline state.[8]

Conjugated molecules with cruciform motifs have received increasing attentions in recent years.[9] Such motifs allow the gradual tuning of inter- and intramolecular interactions, which render them appealing in the development of dual- and even multi-functional materials. For instance, Bunz and coworkers reported three water-soluble and fluorescent aldehyde-substituted distyrylbenzene derivatives with a cruciform structure, showing pH-dependent amine-sensing properties.[10]

In this paper, we report a new cruciform electron donor–acceptor molecule 2,2′-((5,5′-(3,7-dicyano-2,6-bis(dih-exylamino) benzo[1,2-*b*:4,5-*b*′]difuran-4,8-diyl)bis(thiophe-ne-5,2-diyl)) bis(methanylylidene))dimalononitrile (**BDFTM**) (**Scheme 1**). The synthesis of the benzo[1,2-*b*:4,5-*b*′]difuran framework was previously developed by some of us.[11] Through the incorporation of 2-methylenemalononitrile (=$C(CN)_2$) into the thiophene moieties, it was intended to tune the frontier molecular orbital

H. W. Luo, Dr. Z. T. Liu, Dr. C. Zhang, Z. X. Cai, X. Chen, Dr. G. X. Zhang, Prof. Y. S. Zhao, Prof. D. Q. Zhang
Beijing National Laboratory for Molecular Sciences
CAS Key Laboratory of Organic Solids
Institute of Chemistry
Chinese Academy of Sciences
Beijing 100190, PR China
E-mail: drzitong@gmail.com; gxzhang@iccas.ac.cn; dqzhang@iccas.ac.cn

S. J. Chen, Prof. S. Decurtins, Dr. S.-X. Liu
Departement für Chemie und Biochemie
Universität Bern Freiestrasse 3
Bern CH-3012, Switzerland
E-mail: liu@iac.unibe.ch

DOI: 10.1002/adfm.201304027

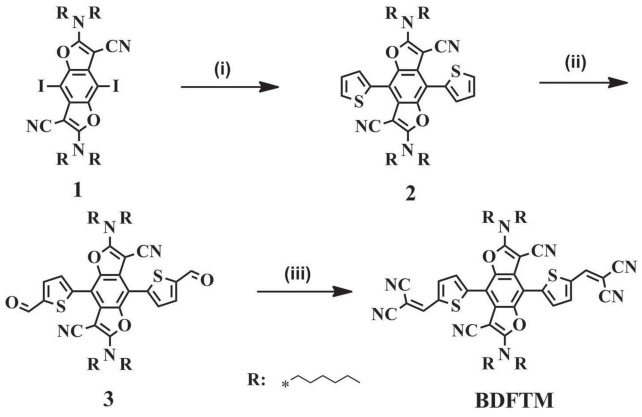


**Scheme 1.** Synthetic route to **BDFTM**. Reagents and conditions: (i) $Pd(pph_3)_4$, toluene, 2-(tributylstannyl)thiophene, reflux, 8 h, 91%; (ii) 1. lithiumdiisopropylamide, –78 °C, 10 min; 2. piperidine-1-carbaldehyde, 1.0 h, 84%; (iii) malononitrile, triethylamine, $CH_2Cl_2$, 2h, 63%.

energies and thus the absorption/emission features. The results reveal that **BDFTM** displays not only relatively strong red emission but also *p*-type semiconducting behavior. Firstly, **BDFTM** is almost non-emissive in solution but it becomes strongly emissive after aggregation. In the solid state, both the red emissive microrods and microplates exhibit outstanding optical waveguide behaviors. Moreover, the crystalline micro-plates are potentially useful as planar optical microcavities. Note that the red emission waveguide materials are seldom reported.[12] Secondly, thin films of **BDFTM** exhibit air stable *p*-type semiconducting behavior with hole mobility up to 0.0015 $cm^2V^{-1}s^{-1}$. Notably, OFETs with thin-films of **BDFTM** can also be employed for highly sensitive and selective detection of $H_2S$; $I_{DS}$, $V_{th}$ and $\mu_h$ are all significantly varied after exposure of the device to $H_2S$, leading to a multiple-parameter sensing of $H_2S$.

## 2. Results and Discussion

### 2.1. Synthesis

The synthesis of the target molecule **BDFTM** starts from compound **1** which was prepared according to the reported procedure.[11] The Stille coupling of **1** with 2-(tributylstannyl) thiophene yielded **2** in 91% yield. Then, compound **2** was allowed to react with lithium diisopropylamide (LDA) at -78 °C, followed by addition of piperidine-1-carbaldehyde, leading to **3** in 84% yield. Finally, **BDFTM** was obtained by the reaction between **3** and malononitrile in the presence of triethylamine in 63% yield. The chemical structure of **BDFTM** was characterized with NMR and MS and its purity was confirmed by elemental analysis. **BDFTM** is thermally stable under 300 °C based on the TGA (thermogravimetric analysis) data shown in Figure S1.

### 2.2. Crystal Structure

**BDFTM** crystallizes in two different morphologies, either as 1D microrods from $CHCl_3$/hexane (v/v, 1:2) or as 2D microplates from $CHCl_3/CH_3OH$ (v/v, 1:2). The microrods and microplates show different X-ray diffraction (XRD) patterns as depicted in Figure S2. The crystals with the rod-like morphology were too small for single crystal X-ray investigation, but the plate-like ones were large enough. The crystal structure with the solvate free plate-like morphology is described in the centrosymmetric triclinic space group P-1, whereby the molecule lies on an inversion center ($Z = 1$). The crystal data are given in Table S1, and the molecular structure as well as the structural packing arrangement are shown in **Figure 1**. Both the 2-(thiophen-2-ylmethylene)malononitrile moiety and the benzo[1,2-*b*:4,5-*b*′] difuran skeleton within **BDFTM** are almost planar, while they form a dihedral angle of 32.7°. The molecules are packed to form a lamellar-like layered structure in which alkyl chains are interdigitated between molecular layers. There are no close intermolecular $\pi$-$\pi$ interactions including those between electron donating and accepting moieties (see Figure 1c). However, molecules interact via C-N...$\pi$ contacts (3.242 Å) between the cyano group on the methylenemalononitrile moitiy and the benzo[1,2-*b*:4,5-*b*′]difuran framework, as depicted in Figure 1e. Furthermore, side-by-side H-bond interactions (C-H...N, 2.362 Å) are observed between the methylenemalononitrile moiety and the cyano group linking to the benzo[1,2-*b*:4,5-*b*′]difuran framework (see Figure 1d). As discussed below, such intermolecular interactions should be responsible for the semiconducting behavior of **BDFTM**. Notably, the lack of intermolecular $\pi$-$\pi$ interactions within the crystal of **BDFTM** can inhibit the formation of excimers and exciplexes, and as a result the compound becomes emissive in the solid state.

### 2.3. HOMO/LUMO Energies

As depicted in **Figure 2**A, **BDFTM** possesses two reversible oxidation waves with $E_{ox1}^{1/2}$ = 0.92 V (vs. Ag/AgCl) and $E_{ox2}^{1/2}$ = 1.25 V. In addition, it exhibits an irreversible reduction wave with $E_{red}^{p}$ = –1.05 V. Based on the onset potentials for the first oxidation and reduction, HOMO and LUMO energies of **BDFTM** were estimated to be –5.26 eV and –3.53 eV, respectively. Accordingly, the bandgap was deduced to be 1.73 eV. Moreover, the HOMO energy matches well with the work function of gold which is employed as drain and source electrodes of OFETs (see below).

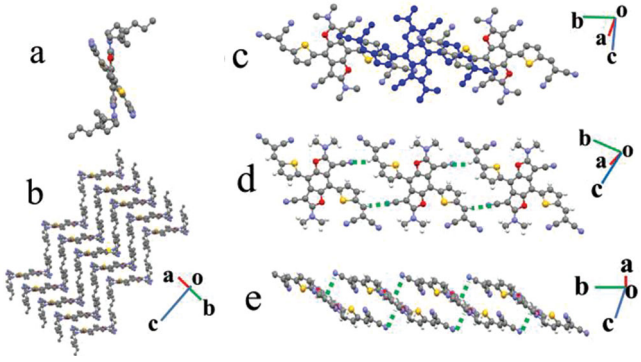


**Figure 1.** Molecular structure and intermolecular arrangements of **BDFTM**; two $-C_6H_{13}$ chains were omitted for the sake of clarity (c–e).

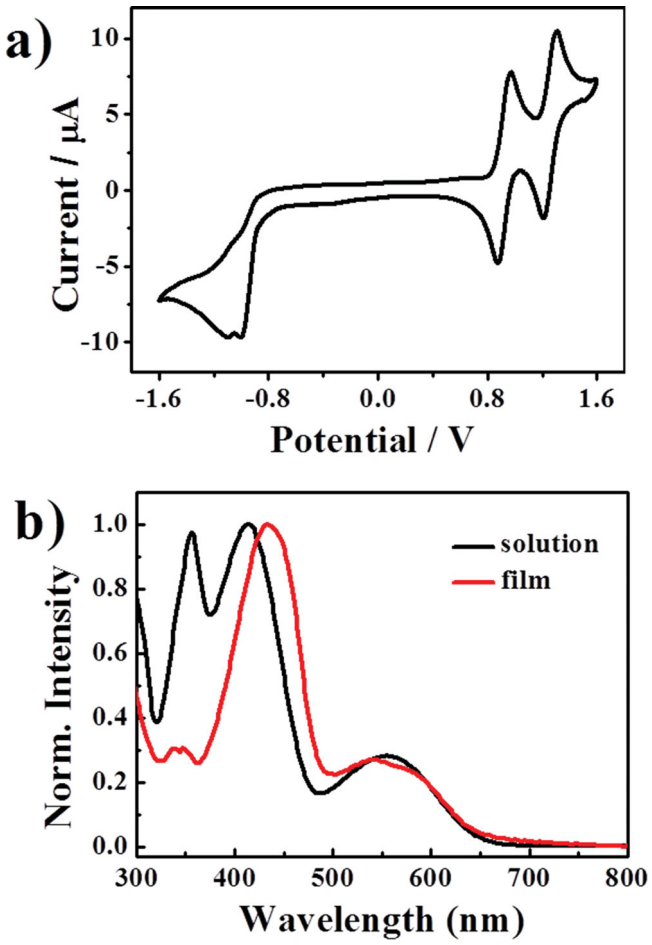


**Figure 2.** (a) Cyclic voltammograms of **BDFTM** (1.0 mM) in $CH_2Cl_2$ solution at a scan rate of 50 $mVs^{-1}$, with Pt as the working and counter electrodes and Ag/AgCl electrode (saturated KCl) as the reference electrode, and *n*-$Bu_4NPF_6$ (0.1 M) as supporting electrolyte. (b) Optical absorption spectra of BDFTM ($1.0 \times 10^{-5}$ M) of a solution in $CH_2Cl_2$ and the film.

The optical absorption spectra of **BDFTM** and its thin film are illustrated in Figure 2B. The compound shows strong absorptions around 356 nm, 414 nm and 554 nm. For the thin film, the absorption around 356 nm is significantly reduced, and that around 414 nm is red-shifted by 20 nm, whereas the low-energy band is slightly blue-shifted. Based on the absorption red-edge, the optical bandgap is estimated to be 1.93 eV, being in good agreement with the electrochemical gap of 1.73 eV.

DFT calculations at the level of B3LYP/6-31G were performed for **BDFTM** (Table S2). The ground-state geometry was optimized with no symmetry constraints. As depicted in **Figure 3**, the HOMO orbital is mainly localized on the benzo[1,2-*b*:4,5-*b*′]difuran framework, whereas the LUMO orbital is distributed on 2-(thiophen-2-ylmethylene)malononitrile fragments. The calculated HOMO and LUMO energies are –5.37 eV and –3.17 eV, respectively. These are different from those obtained with cyclic voltammetric and absorption spectral data. However, this is understandable as solvent effects and intermolecular interactions are not involved in the theoretical calculations.[13]

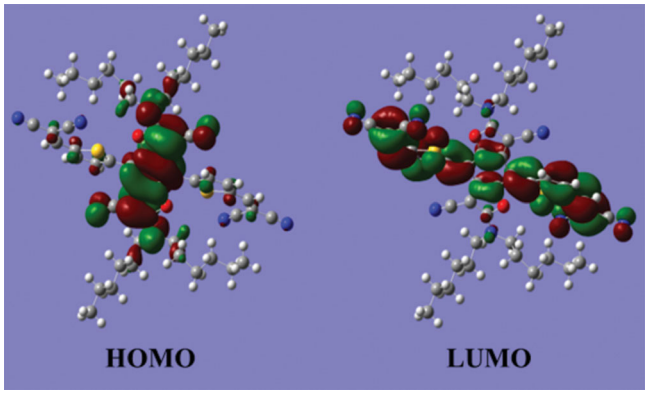


**Figure 3.** HOMO/LUMO orbitals of **BDFTM** based on DFT calculations.

### 2.4. Aggregation-Induced Emission and Optical Waveguiding Behavior of Crystalline Microrods/Microplates

**BDFTM** is almost non-emissive in good solvents such as $CH_2Cl_2$ and THF, however, the fluorescence starts to increase upon addition of *n*-hexane, a poor solvent for **BDFTM** (**Figure 4**). A remarkable fluorescence enhancement is realized when the volume fraction of *n*-hexane reaches 70% and 60% for solvent $CH_2Cl_2$ and THF, respectively. Simultaneously, the fluorescence spectrum is gradually blue-shifted. Based on dynamic light scattering (DLS) data shown in Figure S3, aggregates of ca. 295 nm were formed upon addition of *n*-hexane to the $CH_2Cl_2$ solution of **BDFTM**. Therefore, **BDFTM** exhibits typical aggregation-induced emission.[14,15] This behavior may be ascribed to the fast internal rotations in the excited state around the sigma bonds that connect the conjugated moieties. The slight blue-shift of the emission maximum is probably owing to the fact that **BDFTM** adopts a more twisting conformation after aggregation according to previous reports.[16] The microcrystalline powders of **BDFTM** show strong red emission with a quantum efficiency of 16% and an average fluorescence lifetime ($<\tau>$) of 2.02 ns (see Figure S4).

The emission spectra of the 1D microrods and 2D microplates are slightly different as depicted in Figure S5. The 1D microrods show strong emission around 676 nm, whereas the emission of the 2D microplates is slightly red-shifted with a shoulder around 709 nm. Such emission difference may originate from the different intermolecular arrangements and interactions within the 1D microrods and 2D microplates. **Figure 5** shows the PL images of both microrods and microplates. **Figure 6**a depicts the PL (photoluminescence) image of 1D surface-smooth microrods with a diameter of ca. 2.5 μm. The microrods exhibit intense red emission under UV (365 nm) light excitation. Obviously, bright PL spots are detected at the tips of 1D microrods, whereas the remaining surface shows only a relatively weak red-emission. Such PL images reveal that 1D microrods can function as active optical waveguides, in which PL energy can propagate efficiently along the axial direction, which is in agreement with previous studies.[17] To quantify the light waveguiding efficiency within microrods of **BDFTM**, the spatially resolved PL spectra were collected by locally exciting the sample with a 375 nm laser. Figure 6b shows the collected PL spectra at the end of a single microrod of **BDFTM**

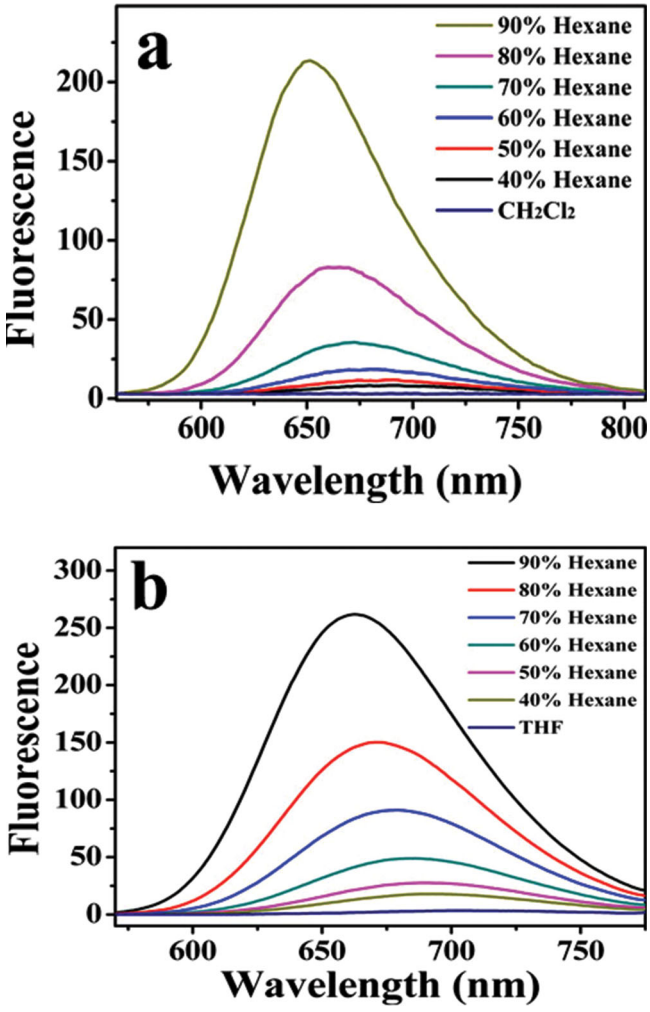


**Figure 4.** Fluorescence spectra of **BDFTM** in $CH_2Cl_2$ (a) and THF (b) and those after addition of different amounts of *n*-hexane; the percentages are volume fractions.

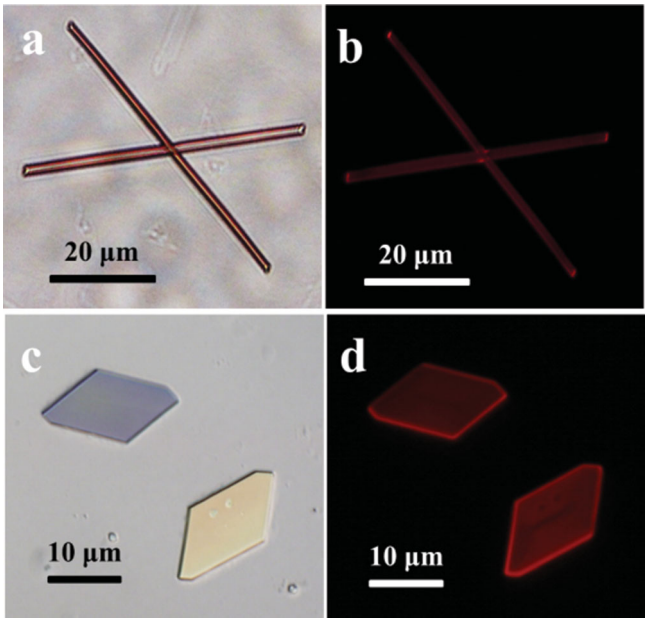


**Figure 5.** a,c) Bright-field and b,d) PL images of the 1D microrods and microplates excited with mercury lamp.

under the excitations at different positions (Figure 6a, labeled as 1–6). Obviously, the emission intensity at the microrod-ends decreases with increasing propagation distance. As depicted in Figure 6c, the peak intensity of the outcoupled light decreases almost exponentially with the propagation distance. By fitting the data of Figure 6c according to the reported procedure,[18] the optical loss coefficient at 676 nm for microrods of **BDFTM** was estimated to be 60 $dBmm^{-1}$, which is lower than most previously reported organic optical waveguides.[12a]

**Figure 7**a shows a PL image of well-defined 2D microplate with edge lengths of 11 μm × 11 μm. The edges show brighter red emission than the respective surfaces of microplates, indicating that efficient light guiding can also occur within 2D microplates of **BDFTM**. As shown in Figure 7b, four edges (marked with 1-4) displayed bright out-coupled red-lights when the laser beam was focused on the center of the microplate. The respective PL spectra of the four edges (marked with 1-4) were measured (see Figure 7c). The emission light intensities of edges 1 and 2 are slightly higher than those of edges 3 and 4. Such slight anisotropic light propagation efficiencies in these 2D microplates may be related to the intermolecular packing direction as the molecular stacking and the direction of the optical transition dipole moment determine the dielectric properties and photon transport abilities.[16]

Note that the bright outcoupled light from the microplate edges implies that the emitted light might be confined by reflection at boundaries. This kind of reflection at each boundary allows for photon confinement in a 2D microplate. The reflection at each edge of the microplate forms a quasi-whispering-gallery-mode (quasi-WGM) optical resonance of the red fluorescence as shown in the high-resolution (~0.16 nm) spectrum in Figure 7d. The optical path $L$ of inner light transport is about 33 μm, estimated by $L = \lambda^2/n\Delta\lambda$, where $\lambda$ is the light wavelength, $\Delta\lambda$ is the mode space between two peaks, and $n$ is the refractive index (around 1.5).[19] The optical path is almost 0.8 times of the circumference of microplate, indicating that the quasi-WGM mode in the planar cavity is based on the inner reflection at four edges of the microplate.

### 2.5. OFET with Thin-Film of BDFTM

The semiconducting behavior of **BDFTM** was investigated by fabrication of thin-film OFETs. The bottom-gate top-contact (BGTC) devices on OTS (octadecyltrichlorosilane) modified Si/$SiO_2$ substrates were fabricated with conventional techniques (see below). Molecules of **BDFTM** were vacuum-deposited at different substrate temperatures (30 °C, 50 °C, 70 °C, and 90 °C) to form the thin films on OTS modified substrates. **Figure 8** shows the typical transfer and output characteristics (measured in air) of an OFET with a thin film of **BDFTM**, which exhibits *p*-type semiconducting behavior as $I_{DS}$ increases by applying negative $V_{GS}$. This agrees well with the HOMO energy (–5.26 eV) of **BDFTM**, whereas the LUMO energy

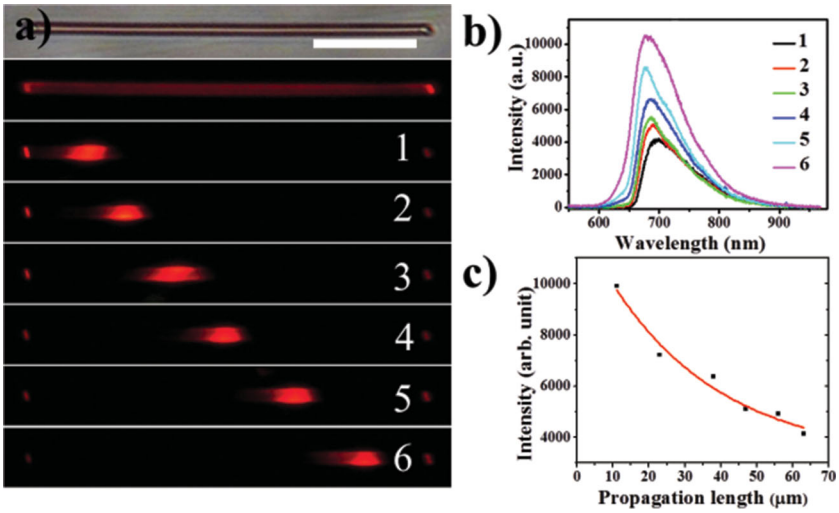


**Figure 6.** a) PL images obtained by exciting an identical microrod at different positions. Scale bar is 20 μm. b) the spatially resolved spectra of the waveguided emission that is outcoupled by excitation at a distance of 63, 56, 47, 38, 23 and 11 μm from the tip of a single nanorod (from 1 to 6 in panel a), and c) the output intensity as a function of propagation length.

(–3.53 eV) is too high to show air-stable *n*-type semiconducting property.

The as-prepared OFET possesses low hole mobility ($3.0 \times 10^{-4}$ $cm^2V^{-1}s^{-1}$), which however increases by elevating the OTS-modified substrate temperature, as listed in **Table 1**. The mobility increases by enhancing the substrate temperature from 30 °C to 70 °C, but it decreases by further increasing the substrate temperature to 90 °C. The hole mobility reached $1.5 \times 10^{-3}$ $cm^2V^{-1}s^{-1}$ when the substrate was heated to 70 °C. The on/off ratio (ca. $10^5$) and threshold voltage (ca. 40 V) remained almost unaltered while varying the substrate temperatures. Notably, the *p*-type semiconducting properties (mobility, on/off ratio and threshold voltage) are air stable and reproducible (Figure S6).

Atomic force microscope (AFM) and XRD studies were performed in order to understand the variation of the thin film morphology and intermolecular packing order upon increasing the substrate temperatures. As depicted in **Figure 9**, the thin film deposited at 30 °C contains interconnected thin microrods which are ca. 1200 nm in length and ca. 160 nm in width. By increasing the substrate temperature, the size of these microrods increases and the microrods transform into layered structures. The interlayer distance is estimated to be 1.61 nm (Figure S7), which is rather close to the length of **BDFTM** along the *c* direction. The formation of such layered structures is beneficial for carrier-transport. However, boundary areas emerge after further increasing the substrate temperature to 90 °C. Such morphological changes are in agreement with the variation of hole

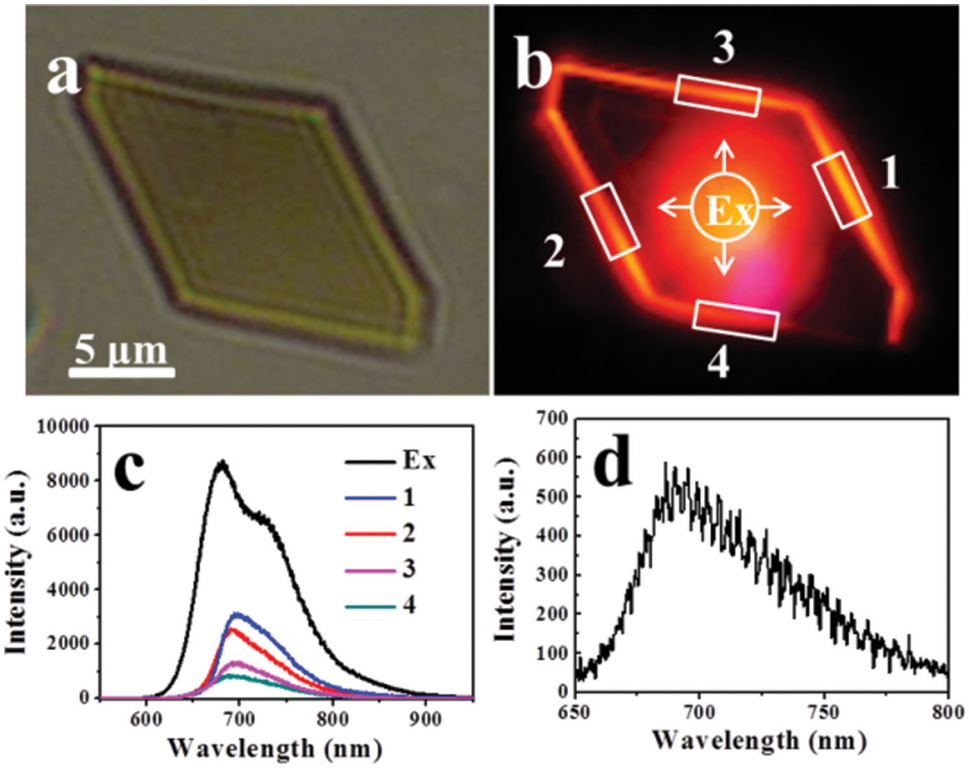


**Figure 7.** a) Bright-field and b) PL images of the microplate. The arrows show the guiding directions. c) The corresponding spatially resolved PL spectra of the excited spot and the four edges (marked with 1–4). d) Modulated PL spectra of the microplate.

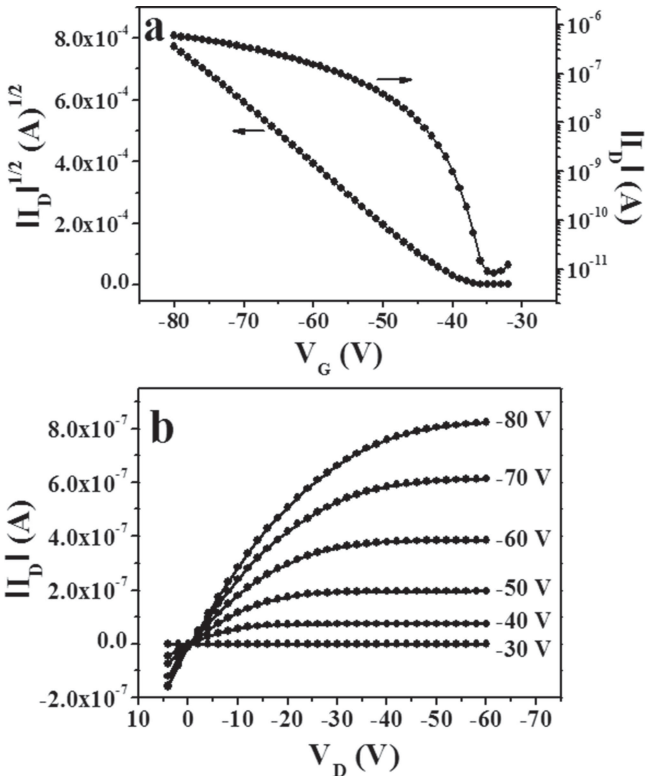


**Figure 8.** Transfer (a) and output (b) characteristics for OFET based on thin-film of **BDFTM** deposited on OTS-modified $SiO_2$/Si substrate at 70 °C.

mobilities of thin films of **BDFTM** as a function of the substrate temperature (see Table 1).

The thin film of **BDFTM** deposited at 30 °C shows only one weak XRD signal at 5.2° (see Figure 9), which is remarkably enhanced and also a new weak diffraction peak appears at 21.7° when deposited at 70 °C. The diffraction signals at 5.2° and 21.7° match well with the corresponding two diffractions of the single crystal of **BDFTM** (see Figure S2). The diffraction signal at 5.2° corresponds to a *d*-spacing of 1.63 nm, which is rather close to the length of BDFTM along *c* direction while the diffraction at 21.7°, corresponding to 4.2 Å, may be associated with short intermolecular contacts (CN...$\pi$). These XRD data agree with the fact that the hole mobility was initially enhanced by increasing the substrate temperature up to 70 °C and then decreased.

### 2.6. OFET-Based Detection of $H_2S$ Gas

In the following, we demonstrate the application of OFETs with thin-films of **BDFTM** in the highly sensitive and selective detection of $H_2S$. **Figure 10**a shows the response of the transfer characteristics for OFET with a thin film of **BDFTM** deposited at 70 °C after exposure to different concentrations of $H_2S$. Obviously, the following parameters are varied: i) on-current (at $V_G$ = –80 V), ii) threshold voltage and iii) hole mobility. As

**Table 1.** Mobility (μ), current on/off ratio ($I_{on}/I_{off}$) and threshold Voltage ($V_T$) of OFETs with thin-films of **BDFTM** at different substrate temperatures.

| T [°C] | μ [$cm^2V^{-1}s^{-1}$] | $I_{on}/I_{off}$ | $V_T$ [V] |
|---|---|---|---|
| 30 | (2.5–3.0) × $10^{-4}$ | $10^4$–$10^5$ | 39–40 |
| 50 | (7.6–8.4) × $10^{-4}$ | $10^5$ | 39–41 |
| 70 | (1.1–1.5) × $10^{-3}$ | $10^5$ | 40–41 |
| 90 | (7.4–8.2) × $10^{-4}$ | $10^5$ | 40-41 |

depicted in Figure 10b, the hole mobility only decreases slightly when the concentration of $H_2S$ is lower than 0.1 ppm. However, the hole mobility is reduced significantly after exposure to high concentrations (>0.1 ppm) of $H_2S$. The threshold voltage increases from 40 V to 41 V after exposure to $H_2S$ with a concentration of 0.1 ppm. Figure 10a also shows the decrease of on-current after exposure of OFET to $H_2S$ gas. For instance, the on-current decreases by 11% after exposure to 0.1 ppm of $H_2S$ gas; this reduction of on-current is still detectable even when the concentration of $H_2S$ is as low as 10 ppb (see Figure S8). Furthermore, the response of on-current vs time upon exposure to $H_2S$ was performed. As shown in Figures 10c and d, the on-current decreases rather quickly after exposure to $H_2S$ and reaches to a stable current within 5.0 s. In comparison, the drain current decreases only slightly and slowly after exposure to air as shown in Figure 10c. Notably, such on-current variations induced by $H_2S$ gas are well reproducible.

The selectivity of the OFET with thin film of **BDFTM** toward $H_2S$ was investigated (**Figure 11**). Volatile solvents such as dichloromethane and hexane and those with nucleophilic reactivities such as acetone, methanol and ammonia ($NH_3$) were selected for the studies. The variation of on-current can be neglected after exposure to these gases (except $NH_3$) at high concentrations (>1000 ppm). However, the decrease of on-current becomes discernible in the presence of 150 ppb of $NH_3$. Nevertheless, the OFET with thin-film of **BDFTM** shows much higher sensitivity toward $H_2S$. Therefore, highly sensitive and selective detection of $H_2S$ gas can be achieved with a thin film OFET of **BDFTM**.

OFET-based sensing is usually based on trapping or doping processes induced by the interactions of gas analytes and semiconducting layers; [20–22] as a result carrier mobilities, on-current

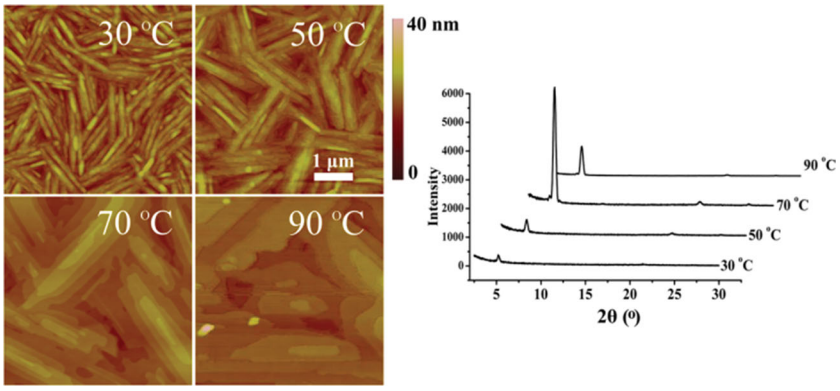


**Figure 9.** AFM images (left) and XRD patterns (right) based on thin-film of **BDFTM** deposited on OTS-modified $SiO_2$/Si substrates after annealing at different temperatures.

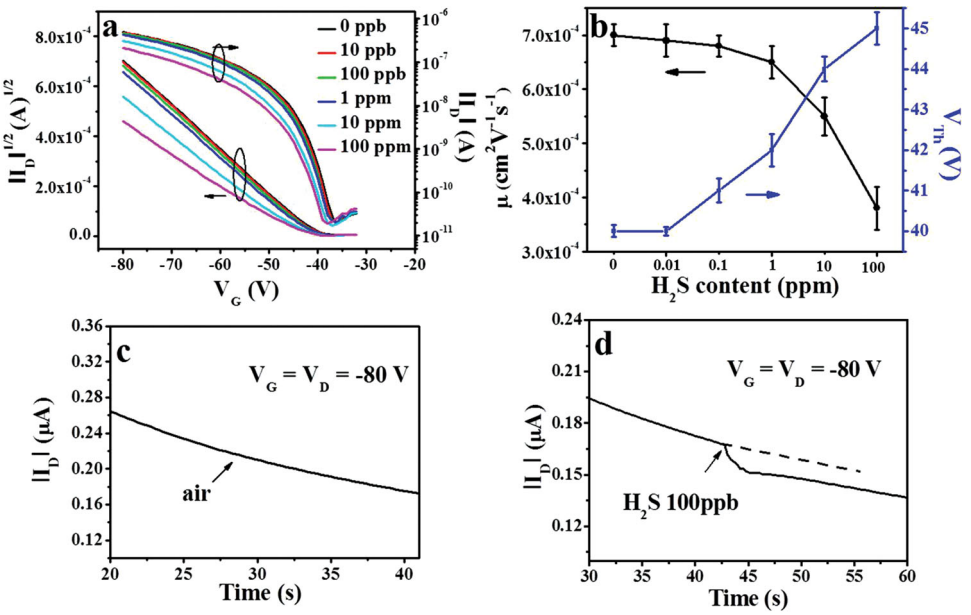


**Figure 10.** (a) Transfer characteristics ($I_{DS}$ vs. $V_G$) and (b) variation of mobility and threshold voltage upon exposure to different concentrations (0–100 ppm) of $H_2S$. (c) Drain current *vs* time under air and (d) 100 ppb concentration of $H_2S$.

($I_{DSAT}$) and other parameters are varied accordingly. However, the selective sensing of $H_2S$ with thin film OFET of **BDFTM** is probably due to the Michael addition of $H_2S$ toward the 2-methylenemalononitrile groups within **BDFTM** (**Scheme 2**). As shown in Figure S9, the signal at $\delta = 7.90$ ppm, which is due to the hydrogens attached to the C=C double bonds in **BDFTM**, disappeared gradually after reaction with $H_2S$ gas. Simultaneously, new signals at $\delta = 2.22$ ppm and 2.01 ppm appeared. In addition, new MS (MALDI-TOF) signals at $m/z$ = 925.1 and 959.2 were detected for the sample of **BDFTM** after exposure to $H_2S$ gas as depicted in Figure S10. These $^1$H NMR and MS data confirm the Michael reaction of **BDFTM** with $H_2S$. This explains well the selectivity of the thin film OFET of **BDFTM** toward to $H_2S$ gas. Since the Michael reaction is irreversible, this OFET-based sensor toward $H_2S$ cannot be re-used. The slight interference from $NH_3$ becomes plausible because $NH_3$ also shows nucleophilic reactivity. In fact, the MS signal at m/z = 907.5 corresponding to the mono-Michael adduct of **BDFTM** with $NH_3$ was detected for **BDFTM** after exposure to $NH_3$ gas (see Figure S11).[23] As a result, we have successfully built up a very sensitive/selective $H_2S$ OFET chemical sensor with detect limitation down to 10 ppb based on **BDFTM**. This result could broaden the application of organic field-effect transistors whose mobilities are much lower than that of monocrystalline silicon and until now still inapplicable in next generation integrated circuits.

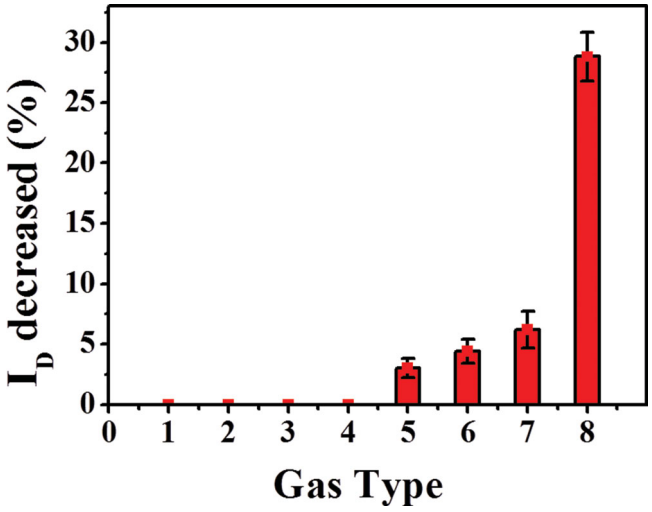


**Figure 11.** Variation of the drain current after exposure to different gas vapors: 1, $H_2$ (pure); 2, $CO_2$ (pure); 3, hexane (52000 ppm); 4, $CH_2Cl_2$ (301000 ppm); 5, $CH_3OH$ (6500 ppm); 6,acetone (1000 ppm); 7, $NH_3$ (150 ppb); 8, $H_2S$ (100 ppb) under the same conditions.

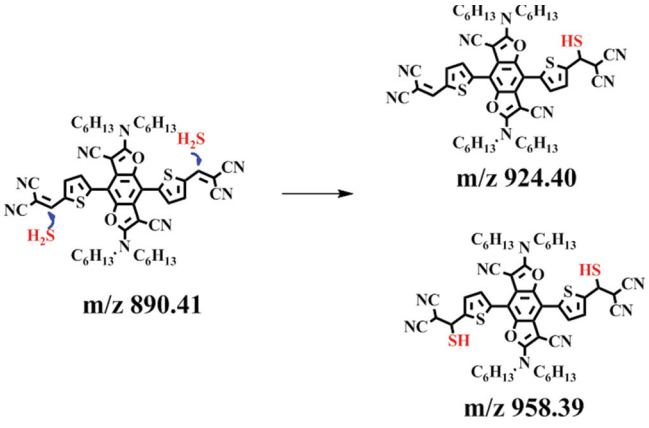


**Scheme 2.** The reaction mechanism of **BDFTM** with $H_2S$.

## 3. Conclusion

In this paper, we report a new cruciform D-A molecule, **BDFTM**, exhibiting both remarkable solid-state red emission and *p*-type semiconducting behavior. **BDFTM** exhibits aggregation-induced emission; it is almost non-emissive in good solvents. Microrods and microplates show typical optical waveguiding behaviors with a rather low optical loss coefficient. Moreover, microplates of **BDFTM** can function as planar optical microcavities which can confine the emitted photons by reflection at the crystal edges. Notably, thin film shows air stable *p*-type semiconducting property with hole mobility up to 0.0015 $cm^2V^{-1}s^{-1}$. The dual functions of **BDFTM** is ascribed to the unique crystal structure of **BDFTM** in which there are no intermolecular face-to-face $\pi$–$\pi$ interactions, but molecules are associated with intermolecular CN...$\pi$ and H-bonding interactions. In addition, hole mobility, threshold voltage and on-current of OFET with thin-film of **BDFTM** are varied after exposure to $H_2S$. Thus, a multi-parameter sensing for $H_2S$ gas is achieved with high sensitivity (down to 10 ppb) along with good selectivity.

## 4. Experimental Section

*Materials and Characterization Techniques*: Chemicals which were purchased from Aldrich, Alfa Aesar, J&K Chemical were used as received without further purification. All solvents were purified and dried following standard procedures unless otherwise stated. Compound **1** was prepared according to the reported procedure.[11]

Melting point was measured with a BÜCHI B-540 microscope apparatus. $^1$H-NMR and $^{13}$C-NMR spectra were recorded on BrukerAvance 400, Avance 300 spectrometers. TOF-MS spectra were determined with a BEFLEX III spectrometer. Elemental analyses were performed on a Carlo-Erba-1106 instrument. Electronic absorption spectra were determined used a Jasco V570 UV-vis spectrophotometer. Cyclic voltammetric measurements were performed in a standard three-electrode cell, with Pt/C as the working electrode and Pt as auxiliary electrode, and Ag/AgCl electrode (saturated KCl) as the reference electrode; *n*-$Bu_4NPF_6$ (0.1 mol/L) was used as supporting electrolyte. TGA analyses were performed on a Shaimdzu DTG-60 instruments under a dry $N_2$ flow at a heating rate of 10 °C/min, heating from room temperature to 550 °C. X-ray diffraction (XRD) measurements were carried out in the reflection mode using a Rigaku D/max-2500 X-ray diffractometer. AFM images were recorded on a Nanoscope III atomic force microscopy (AFM) in trapping mode.

*Crystal Structural Analysis*: Crystals of **BDFTM** were grown by slow evaporation from CHCl3/CH3OH (v/v = 1:1) solutions. All single crystal data were collected on a Rigaku Saturn diffractometer with CCD area detector. All calculations were performed using the SHELXL97 and crystal structure crystallographic software packages. Crystallographic data (excluding structure factors) for the structure of BDFTM in this paper have been deposited with the Cambridge Crystallographic Data Centre as supplementary publication no. CCDC: 938514

*Synthesis of Compound* **2**: Under nitrogen atmosphere, a solution of compound **1** (1.0 g, 1.2 mmol), 2-(tributylstannyl)thiophene (940 mg, 2.52 mmol) and tetrakis(triphenylphosphine)palladium (2%) in toluene (50 mL) was refluxed for 8.0 h. The solvent was removed under reduced pressure. The crude product was purified by silica gel chromatography with $CH_2Cl_2$/petroleum ether (v/v, 1:1) as eluent. Compound **2** was obtained as a yellow solid (800 mg) in 91% yield. $^1$H NMR (300 MHz, $CDCl_3$, $\delta$): 7.49 (d, $J$ = 5.0 Hz, 2H), 7.36 (d, $J$ = 3.3 Hz, 2H), 7.21 (t, $J_1$ = 4.9 Hz, $J_2$ = 3.7 Hz, 2H), 3.52 (t, $J$ = 7.6 Hz, 8H), 1.69 (br, 8H), 1.31 (br, 24H), 0.89 (t, $J$ = 6.4 Hz, 12H); $^{13}$C NMR (75 MHz, $CDCl_3$, $\delta$): 163.6, 143.1, 131.2, 129.7, 126.5, 126.5, 121.6, 116.4, 107.6, 61.7, 50.0, 31.4, 28.4, 26.0, 22.5, 13.9; MS (MALDI-TOF) $m/z$: [M$^+$] calcd for $C_{44}H_{58}N_4O_2S_2$, 738.4; found 738.7; Anal. calcd for $C_{44}H_{58}N_4O_2S_2$: C 71.50, H 7.91, N 7.58, S 8.68; found: C 71.41, H 7.90, N 7.60, S, 8.48.

*Synthesis of Compound* **3**: A solution of lithium diisopropylamide (0.29 mL, 2.0 M in hexane) was added dropwise at -78 °C to a solution of **2** (200 mg, 0.27 mmol) in dry THF (20 ml) under nitrogen atmosphere. After 10 min, piperidine-1-carbaldehyde (68 mg, 0.60 mmol) was added and stirring continued for 1.0 h. The reaction mixture was quenched with $H_2O$ (0.5 mL), washed with $H_2O$ (20 mL × 3), and then dried with anhydrous $Na_2SO_4$. The solvent was removed under reduced pressure. The crude product was purified by silica gel chromatography with $CH_2Cl_2$ as eluent. Compound **3** (170 mg) was obtained as a yellow solid in 84% yield. $^1$H NMR (400 MHz, $CDCl_3$, $\delta$): 9.97 (s, 2H), 7.86 (d, $J$ = 3.6 Hz, 2H), 7.46 (d, $J$ = 3.6 Hz, 2H), 3.53 (t, $J$ = 7.2 Hz, 8H), 1.69 (br, 8H), 1.29 (br, 24H), 0.87 (s, 12H); $^{13}$C NMR (100 MHz, $CDCl_3$, $\delta$): 183.0, 163.9, 144.6, 142.9, 140.8, 135.9, 131.3, 121.6, 116.3, 107.4, 61.8, 50.5, 31.6, 28.6, 26.2, 22.6, 14.0; MS (MALDI-TOF) $m/z$: [M$^+$] calcd for $C_{46}H_{58}N_4O_4S_2$, 794.4; found 794.2; Anal. calcd for $C_{46}H_{58}N_4O_4S_2$: C 69.49, H 7.35, N 7.05, S 8.07; found: C 69.35, H 7.41, N 7.10, S, 7.95.

*Synthesis of* **BDFTM**: In 20 mL of $CH_2Cl_2$, compound **3** (100 mg, 0.13 mmol), malononitrile (18 mg, 0.27 mmol) and triethylamine (two drops) were stirred for 2.0 h. The solvent was removed under reduced pressure. After separation by column chromatography on silica gel with $CH_2Cl_2$ as eluent, **BDFTM** was obtained as a red solid in 63% yield. mp 208.1-209.5 °C ; $^1$H NMR (300 MHz, $CDCl_3$, $\delta$): 7.90 (s, 2H), 7.82 (d, $J$ = 2.1 Hz, 2H), 7.52 (d, $J$ = 2.4 Hz, 2H), 3.58 (t, $J$ = 6.6 Hz, 8H), 1.71 (br, 8H), 1.30 (br, 24H), 0.87 (br, 12H); $^{13}$C NMR (75 MHz, $CDCl_3$, $\delta$): 163.9, 150.8, 142.8, 142.7, 138.5, 136.2, 131.7, 121.6, 113.9, 113.1, 106.9, 77.9, 50.3, 31.4, 28.4, 26.1, 22.6, 14.0; MS (MALDI-TOF) $m/z$: [M$^+$] calcd for $C_{52}H_{58}N_8O_2S_2$, 890.4; found 890.8; Anal. calcd for $C_{52}H_{58}N_8O_2S_2$: C 70.08, H 6.56, N 12.57, S 7.20; found: C 70.27, H 6.64, N 12.64, S, 7.19.

*OFET Fabrication and Characterization*: OFETs were fabricated with a bottom-contact configuration. A *n*-type Si wafer with a $SiO_2$ layer of 500 nm and a capacitance of 9.0 $nFcm^{-2}$ was used as the gate and dielectric. Molecules of **BDFTM** (about 30 nm in thickness) were vacuum deposited (0.1 Å/s) on octadecyltrichlorosilane(OTS)-modified Si/$SiO_2$ substrate at different substrate temperatures (30 °C, 50 °C, 70 °C and 90 °C). And gold source and drain contacts (30 nm) were deposited on the organic layer through a shadow mask. The channel width/length (W/L) ratio was 110. The measurements were carried out under ambient atmosphere at room temperature using a Keithley 4200 SCS semiconductor parameter analyzer. The mobility was extracted from the following equation:

$$I_{DS} = (W/2L)C_i\mu(V_{GS}-V_T)^2$$

where $\mu$ is the field-effect mobility, $L$ and $W$ are the channel length and width, respectively, $C_i$ is the insulator capacitance per unit area, and $V_{GS}$ and $V_T$ is the gate voltage and threshold voltage, respectively.

*Photophysical Studies*: To measure the microarea PL spectra of single microrod, the microrods dispersed on a glass cover-slip were excited with a mercury lamp. Quantum efficiencies of **BDFTM** in the solid states (microcrystalline powders) were recorded on Fluoromax-4 spectrofluorometer with a calibrated integrating sphere system. Fluorescence lifetimes of **BDFTM** were measured based on time-resolved PL experiments which were made with a regenerative amplified Ti: sapphire laser (Spectra-Physics, Spitfire) at 485 nm (150 fs pulse width, second harmonic). The PL spectra were recorded with a streak camera (C5680, Hamamatsu Photonics) attached to a polychromator (Chromex, Hamamatsu Photonics), with the temporal and spectral resolutions of the detector of ca. 10 ps and 2.0 nm, respectively. All the spectroscopic measurements were carried out at room temperature.

## Supporting Information

Supporting Information is available from the Wiley Online Library or from the author.

## Acknowledgements

The present research was financially supported by NSFC(21372226), the State Basic Program and Chinese Academy of Sciences, the Swiss National Science Foundation (Grant No 200021-147143) and the Sino-Swiss Science and Technology Cooperation.

Received: November 30, 2013
Revised: February 15, 2014
Published online: April 2, 2014

[1] a) H. J. Son, L. Y. Lu, W. Chen, T. Xu, T. Y. Zheng, B. Carsten, J. Strzalka, S. B. Darling, L. X. Chen, L. P. Yu, *Adv. Mater.* **2013**, *25*, 838; b) M. Kim, J. N. Hohman, H. Ma, A. K.-Y. Jen, P. S. Weiss, *Science* **2011**, *331*, 1312; c) H. Usta, A. Facchetti, T. J. Marks, *Acc. Chem. Res.* **2011**, *44*, 501; d) T. Sakanoue, H. Sirringhaus, *Nat. Mater.* **2010**, *9*, 736; e) Y. Y. Liang, L. P. Yu, *Acc. Chem. Res.* **2010**, *43*, 1227; f) S. G. Hahm, Y. Rho, J. Jung, S. H. Kim, T. Sajoto, F. S. Kim, S. Barlow, C. E. Park, S. A. Jenekhe, S. R. Marder, M. Ree, *Adv. Funct. Mater.* **2013**, *23*, 2060.

[2] a) J. Youn, G. R. Dholakia, H. Huang, J. W. Hennek, A. Facchetti, T. J. Marks, *Adv. Funct. Mater.* **2012**, *22*, 1856; b) M. C.-L. Yeung, V. W.-W. Yam, *Chem. Sci.* **2013**, *4*, 2928; c) J. Fan, J. D. Yuen, W. B. Cui, J. Seifter, A. R. Mohebbi, M. F. Wang, H. Q. Zhou, A. Heeger, F. Wudl, *Adv. Mater.* **2012**, *24*, 6164; d) I. Mcculloch, M. Heeney, C. Bailey, K. Genevicius, I. Macdonald, M. Shkunov, D. Sparrowe, S. Tierney, R. Wagner, W. M. Zhang, M. L. Chabinyc, R. J. Kline, M. D. Mcgehee, M. F. Toney, *Nat. Mater.* **2006**, *5*, 328.

[3] a) Z. X. Cai, Y. L. Guo, S. F. Yang, Q. Peng, H. W. Luo, Z. T. Liu, G. X. Zhang, Y. Q. Liu, D. Q. Zhang, *Chem. Mater.* **2013**, *25*, 471; b) T. Lei, Y. Cao, X. Zhou, Y. Peng, J. Bian, J. Pei, *Chem. Mater.* **2012**, *24*, 1762; c) F. J. Zhang, Y. B. Hu, T. Schuettfort, C.-A. Di, X. K. Gao, C. R. McNeill, L. Thomsen, S. C. B. Mannsfeld, W. Yuan, H. Sirringhaus, D. B. Zhu, *J. Am. Chem. Soc.* **2013**, *135*, 2338; d) D. K. Hwang, R. R. Dasari, M. Fenoll, V. Alain-Rizzo, A. Dindar, J. W. Shim, N. Deb, C. Fuentes-Hernandez, S. Barlow, D. G. Bucknall, P. Audebert, S. R. Marder, B. Kippelen, *Adv. Mater.* **2012**, *24*, 4445; e) H. Minemawari, T. Yamada, H. Matsui, J. Tsutsumi, S. Haas, R. Chiba, R. Kumai, T. Hasegawa, *Nature* **2011**, *475*, 364; f) K. Takimiya, S. Shinamura, I. Osaka, E. Miyazaki, *Adv. Mater.* **2011**, *23*, 4347.

[4] a) C. L. Wang, H. L. Dong, W. P. Hu, Y. Q. Liu, D. B. Zhu, *Chem. Rev.* **2012**, *112*, 2208; b) S. H. Dong, H. T. Zhang, L. Yang, M. L. Bai, Y. Yao, H. L. Chen, L. Gan, T. Y. Yang, H. Jiang, S. M. Hou, L. J. Wan, X. F. Guo, *Adv. Mater.* **2012**, *24*, 5576; c) S. H. Wang, M. Kappl, I. Liebewirth, M. Müller, K. Kirchhoff, W. Pisula, K. Müllen, *Adv. Mater.* **2012**, *24*, 417; d) L. Q. Li, L. Jiang, W. C. Wang, C. Du, H. Fuchs, W. P. Hu, L. F. Chi, *Adv. Mater.* **2012**, *24*, 2159.

[5] a) S. Holliday, J. E. Donaghey, I. McCulloch, *Chem. Mater.* 2014, DOI: 10.1021/cm402421p; b) G. Giri, E. Verploegen, S. C. B. Mannsfeld, S. Atahan-Evrenk, D. H. Kim, S. Y. Lee, H. A. Becerril, A. Aspuru-Guzik, M. F. Toney, Z. N. Bao, *Nature* **2011**, *480*, 504; c) Z. X. Liang, Q. Tang, J. B. Xu, Q. A. Miao, *Adv. Mater.* **2011**, *13*, 1535; d) H. Sirringhaus, *Adv. Mater.* **2009**, *21*, 3859.

[6] a) Z. K. Wang, S. J. Chen, J. W. Y. Lam, W. Qin, R. T. K. Kwok, N. Xie, Q. L. Hu, B. Z. Tang, *J. Am. Chem. Soc.* **2013**, *135*, 8238; b) Q. M. Peng, W. J. Li, S. T. Zhang, P. Chen, F. Li, Y. G. Ma, *Adv. Opt. Mater.* **2013**, *5*, 362; c) Y. S. Zhao, H. B. Fu, A. D. Peng, Y. Ma, Q. Liao, J. N. Yao, *Acc. Chem. Res.* **2010**, *43*, 409.

[7] a) H. Uoyama, K. Goushi, K. Shizu, H. Nomura, C. Adachi, *Nature* **2012**, *492*, 234; b) K. K. Kartha, S. S. Babu, S. Srinivasan, A. Ajayaghosh, *J. Am. Chem. Soc.* **2012**, *134*, 4834; c) S. Mahesh, A. Gopal, R. Thirumalai, A. Ajayaghosh, *J. Am. Chem. Soc.* **2012**, *134*, 7227; d) D. Chaudhuri, D. B. Li, Y. Che, E. Shafran, J. M. Gerton, L. Zang, J. M. Lupton, *Nano Lett.* **2011**, *11*, 488; e) M. Law, D. J. Surbuly, J. C. Johnson, J. Goldberger, R. J. Saykally, P. Yang, *Science* **2004**, *305*, 1269.

[8] A. Dadvand, A. G. Moiseev, K. Sawabe, W. H. Sun, B. Djukic, I. Chung, T. Takenobu, F. Rosei, D. F. Perepichka, *Angew. Chem. Int. Ed.* **2012**, *51*, 3837.

[9] a) M. N. Gard, A. J. Zucchero, G. Kuzmanich, C. Oelsner, D. Guldi, A. Dreuw, U. H. F. Bunz, M. A. Garcia-Garibay, *Org. Lett.* **2012**, *14*, 1000; b) E. A. Davey, A. Zucchero, O. Trapp, U. H. F. Bunz, *J. Am. Chem. Soc.* **2011**, *133*, 7716; c) J. A. Marsden, J. J. Miller, L. D. Shirtcliff, M. M. Haley, *J. Am. Chem. Soc.* **2005**, *127*, 2464.

[10] F. Freudenberg, J. Kumpf, V. Schäfer, E. Sauter, S. J. Wörner, K. Brödner, A. Dreuw, U. H. F. Bunz, *J. Org. Chem.* **2013**, *78*, 4949.

[11] a) C. Yi, C. Blum, M. Lehmann, S. Keller, S.-X. Liu, G. Frei, A. Neels, J. Hauser, S. Schürch, S. Decurtins, *J. Org. Chem.* **2010**, *75*, 3350; b) H. Li, P. Jiang, C. Yi, C. Li, S.-X. Liu, S. Tan, B. Zhao, J. Braun, W. Meier, T. Wandlowski, S. Decurtins, *Macromolecules* **2010**, *43*, 8058.

[12] a) Z. H. Guo, T. Lei, Z. X. Jin, J. Y. Wang, J. Pei, *Org. Lett.* **2012**, *15*, 3530; b) T. Liu, Y. Li, Y. Yan, Y. Li, Y. Yu, N. Chen, S. Chen, C. Liu, Y. Zhao, H. Liu, *J. Phys. Chem. C* **2012**, *116*, 14134; c) Y. Che, X. Yang, K. Balakrishnan, J. Zuo, L. Zang, *Chem. Mater.* **2009**, *21*, 2930.

[13] X. Chen, J. G. Wang, G. X. Zhang, Z. T. Liu, W. Xu, D. Q. Zhang, *New J. Chem.* **2013**, *37*, 1720.

[14] a) J. D. Luo, Z. L. Xie, J. W. Y. Lam, L. Cheng, H. Y. Chen, C. F. Qiu, H. S. Kwok, X. W. Zhan, Y. Q. Liu, D. B. Zhu, B. Z. Tang, *Chem. Commun.* **2001**, 1740; b) K. Pei, Y. Z. Wu, A. Islam, Q. Zhang, L. Y. Han, H. Tian, W. H. Zhu, *Appl. Mater. Interfaces* **2013**, *11*, 4986; c) B. K. An, J. Gierschner, S. Y. Park, *Acc. Chem. Res.* **2012**, *45*, 544; d) H. N. Kim, Z. Q. Guo, W. H. Zhu, J. Yoon, H. Tian, *Chem. Soc. Rev.* **2011**, *40*, 79; e) L. P. Heng, X. Y. Wang, D. L. Tian, J. Zhai, B. Z. Tang, L. Jiang, *Adv. Mater.* **2010**, *22*, 4716.

[15] a) X. G. Gu, G. X. Zhang, Z. Wang, W. W. Liu, L. Xiao, D. Q. Zhang, *Analyst* **2013**, *138*, 2427; b) X. Shen, G. X. Zhang, D. Q. Zhang, *Org. Lett.* **2012**, *14*, 174; c) X. H. Huang, X. G. Gu, G. X. Zhang, D. Q. Zhang, *Chem. Commun.* **2012**, *48*, 12195; d) Z. T. Liu, W. X. Xue, Z. X. Cai, G. X. Zhang, D. Q. Zhang, *J. Mater. Chem.* **2011**, *21*, 14487; e) M. Wang, G. X. Zhang, D. Q. Zhang, D. B. Zhu, B. Z. Tang, *J. Mater. Chem.* **2010**, *20*, 1858.

[16] a) X. G. Gu, J. J. Yao, G. X. Zhang, D. Q. Zhang, *Small* **2012**, *8*, 3406; b) X. G. Gu, J. J. Yao, G. X. Zhang, Y. L. Yan, C. Zhang, Q. Peng, Q. Liao, Y. S. Wu, Z. Z. Xu, Y. S. Zhao, H. B. Fu, D. Q. Zhang, *Adv. Funct. Mater.* **2012**, *22*, 4862.

[17] a) W. Yao, Y. L. Yan, L. Xue, C. Zhang, G. P. Li, Q. D. Zheng, Y. S. Zhao, H. Jiang, J. N. Yao, *Angew. Chem. Int. Ed.* **2013**, *52*, 8713; b) C. Zhang, Y. L. Yan, Y. Y. Jing, Q. Shi, Y. S. Zhao, J. N. Yao, *Adv. Mater.* **2012**, *24*, 1703.

[18] S. H. Chen, N. Chen, Y. L. Yan, T. F. Liu, Y. W. Yu, Y. J. Li, H. B. Liu, Y. S. Zhao, Y. L. Li, *Chem. Commun.* **2012**, *48*, 9011.

[19] C. Zhang, C. L. Zou, Y. L. Yan, R. Hao, F. W. Sun, Z. F. Han, Y. S. Zhao, J. N. Yao, *J. Am. Chem. Soc.* **2011**, *133*, 7276.

[20] W. G. Huang, K. Besar, R. LeCover, A. M. Rule, P. N. Breysse, H. E. Katz, *J. Am. Chem. Soc.* **2012**, *134*, 14650.

[21] X. Li, Y. D. Jing, G. Z. Xie, H. L. Tai, P. Sun, B. Zhang, *Sens. Actuat. B* **2013**, *176*, 1191.

[22] C. A. Di, F. J. Zhang, D. B. Zhu, *Adv. Mater.* **2012**, *25*, 313.

[23] The selectivity of thin-film OFET toward $H_2S$ is probably owing to the fact that $H_2S$ is more reactive toward 2-methylenemalononitrile groups than $NH_3$.